Human Molecular Genetics, 2017, Vol. 26, No. 16 3069–3080

doi: 10.1093/hmg/ddx191
Advance Access Publication Date: 19 May 2017
Original Article

ORIGINAL ARTICLE

Gene co-expression network analysis for identifying modules and functionally enriched pathways in SCA2

Lance T. Pflieger[1], Warunee Dansithong[2], Sharan Paul[2], Daniel R. Scoles[2], Karla P. Figueroa[2], Pratap Meera[3], Thomas S. Otis[3], Julio C. Facelli[1] and Stefan M. Pulst[2,*]

[1]Department of Biomedical Informatics [2]Department of Neurology, University of Utah, Salt Lake City, UT 84112, USA and [3]Department of Neurobiology, University of California Los Angeles, Los Angeles, CA, USA

*To whom correspondence should be addressed at: Department of Neurology, Clinical Neurosciences Center, 175 North Medical Drive East, Salt Lake City, UT 84132, USA. Tel: +18015856387; Fax: +18015814192; Email: stefan.pulst@hsc.utah.edu

Abstract

Spinocerebellar ataxia type 2 (SCA2) is an autosomal dominant neurodegenerative disease caused by CAG repeat expansion in the *ATXN2* gene. The repeat resides in an encoded region of the gene resulting in polyglutamine (polyQ) expansion which has been assumed to result in gain of function, predominantly, for the ATXN2 protein. We evaluated temporal cerebellar expression profiles by RNA sequencing of ATXN2^{Q127} mice versus wild-type (WT) littermates. ATXN2^{Q127} mice are characterized by a progressive motor phenotype onset, and have progressive cerebellar molecular and neurophysiological (Purkinje cell firing frequency) phenotypes. Our analysis revealed previously uncharacterized early and progressive abnormal patterning of cerebellar gene expression. Weighted Gene Coexpression Network Analysis revealed four gene modules that were significantly correlated with disease status, composed primarily of genes associated with GTPase signaling, calcium signaling and cell death. Of these genes, few overlapped with differentially expressed cerebellar genes that we identified in *Atxn2*$^{-/-}$ knockout mice versus WT littermates, suggesting that loss-of-function is not a significant component of disease pathology. We conclude that SCA2 is a disease characterized by gain of function for ATXN2.

Introduction

Spinocerebellar ataxia type 2 (SCA2) is among the progressive neurodegenerative polyglutamine (polyQ) diseases. It is caused by a CAG repeat expansion in an encoded region of the *ATXN2* gene giving rise to an expanded polyQ domain in the encoded ATXN2 protein (1). Other polyQ/CAG triplet repeat expansion diseases include SCA1, SCA3, SCA6, SCA7, SCA8, SCA12, SCA17, Huntington's disease, spinal bulbar muscular dystrophy and dentatorubral-pallidoluysian atrophy (DRPLA). SCA2 is an autosomal dominant disorder characterized by symptoms resulting from neurodegeneration of cerebellar Purkinje cells (PCs), and neuropathology in the brainstem and spinal cord. SCA2 patients are characterized by progressive loss of coordination, unstable gait, slow saccades and dysarthria (2). There exists no treatment for SCA2.

Multiple transgenic mouse models have been generated to elucidate the role of ATXN2 in neurodegeneration as well as for testing of experimental therapeutics for SCA2 (3–5). The ATXN2^{Q127} mouse model contains 127 CAG repeats in the full-length *ATXN2* cDNA under the control of the PC targeted *Pcp2* promoter. ATXN2^{Q127} mice have onset of motor function deficits as early as 8 weeks, preceded by electrophysiological changes at 6 weeks and gene expression changes at 4 weeks. The observed gene expression changes were identified by relying on a set of established PC marker genes, such as *Calb1* and *Pcp2*, suggesting that earlier and meaningful expression changes may occur prior to dysregulation of PC marker genes. In contrast to ATXN2^{Q127}

Received: February 8, 2017. **Revised:** April 22, 2017. **Accepted:** May 11, 2017

transgenic mice, an Atxn2-CAG42 knock-in mouse model displays no overt ataxic behavior, with the exception of homozygous knock-in animals at 18 weeks, which were associated with deficiency in the cerebellar expression of *Pabpc1* (6). Cerebellar transcriptomes determined by microarray analysis of symptomatic Atxn2-CAG42 knock-in mice revealed few mRNA changes compared with wild-type (WT) mice, including no significant change for the PC marker gene *Calb1*. Two *Atxn2* knock-out mouse lines have also been characterized (7,8). Features of *Atxn2* knock-out mice include obesity, dyslipidemia, insulin resistance, and abnormal fear-related behaviors (9).

To molecularly characterize SCA2 disease progression, we analyzed RNA-sequencing data produced using the cerebella of ATXN2^{Q127} mice collected at three distinct time points. These time points represented cerebellar developmental, prepathological and early disease developmental stages, and were selected to employ a rigorous systems biology approach of analysis to our study that would lead to the identification of functional pathways involved in development of the SCA2 prepathological brain as well as SCA2 disease onset and progression (10,11). Using weighted gene co-expression network analysis (WGNCA), we identified multiple modules associated with disease progression including a module enriched for PC transcripts and a module indicative of cell death. Additionally, we provide a comparison with *Atxn2*$^{-/-}$ mice showing little overlap between the two models, as well as surprisingly few significantly changed genes in *Atxn2* knockout mice versus WT littermates.

Results

Temporal differential expression analysis of ATXN2^{Q127} mice

SCA2 mice are characterized by progressive worsening of molecular, motor and physiological phenotypes, with the earliest biochemical changes detected at 4 weeks of age, as described in Hansen *et al.* (3). To further describe the SCA2 mouse molecular phenotype and its progression, we analyzed gene expression by RNA sequencing of cerebellar tissues from ATXN2^{Q127} and age matched WT mice. Cerebellar tissues were collected at 3 time points: an early developmental stage (age 1 day), a prepathological stage (age 3 weeks) and a stage where electrophysiological changes are detectable (age 6 weeks). RNA libraries were generated from multiple biological replicates from each group and subsequently sequenced on an Illumina HiSeq platform. We identified 146, 458 and 445 differentially expressed genes (DEGs) relative to WT at the day 1, week 3 and week 6 time points, respectively (fold change ≥ 1.5 or ≤ -1.5, *P*-value < 0.01). A larger number of genes had greater fold changes in expression occurring at later time points (Supplementary Material, Table S1). Of the significant DEGs, few were shared across all time points, with the greatest percentage of shared genes occurring between weeks 3 and 6 (Fig. 1).

Enrichment analysis

Gene ontology (GO) and KEGG pathway analysis using DAVID showed that the shared genes between weeks 3 and 6 were strongly enriched for annotations in biological process (BP) and molecular functions related to calcium ion binding and protein binding (12,13). In contrast to the genes shared between day 3 and week 6, the shared genes between weeks 1 and 3 showed strong enrichment for functions in cell growth and regulation. Day 1 and week 6 shared genes showed few relevant enrichment categories (Supplementary Material, Table S2). Globally, stronger changes in down-regulated genes were seen compared with up-regulated genes at each time point (Fig. 1). GO analysis of the significantly down- and up-regulated genes at each time point showed that terms related to calcium ion binding were significantly enriched for the down-regulated genes across all time points, with each time point increasing in significance (Supplementary Material, Table S2). At week 3, BP terms related to developmental processes were significantly enriched for down-regulated genes. Terms related to apoptosis became significantly enriched for up-regulated genes in week 6, whereas down-regulated genes were strongly enriched for terms related to ion transport, PC development and cell signaling.

PC-specific genes are down-regulated in cerebella of SCA2 mice

Top-ranked down-regulated genes at week 6 included multiple previously identified PC markers such as *Trpc3*, *Garnl3*, *Doc2b* and *Dner* (ranked 4th, 10th, 18th and 22nd, respectively). Of the list of known annotated PC marker genes provided by Rong *et al.* (14), 7/30 were down-regulated at week 3, increasing to 23/30 by week 6. None of the 30 marker genes were differentially expressed at day 1 (Supplementary Material, Table S3). The PC marker genes that were down-regulated early, at 3 weeks of age, included *Atp2a3, Cacna1g, Dner, Doc2b, Fgf7, Garnl3* and *Pcp2*.

Up-regulated genes

Across the time points, the number of down-regulated DEGs far exceeded the number of up-regulated DEGs. Specifically at the 3 and 6 week time points, only 97 out of 454 and 130 out of 434 were up-regulated, respectively. Only *Casp3, Adcyap1, Coch, Pappa* and *Mbl2* were significantly up-regulated at 3 and 6 weeks with the cut-offs used for this analysis. Of note, both Casp3 and Adcyap1 are key in cellular response to stress. Also, *Mbl2* was the top up-regulated gene at week 3 and the second most up-regulated gene at week 6. The *Mbl2* gene encodes for mannose binding lectin which has been shown to bind amyloid β peptides (15).

Weighted gene co-expression network analysis

To gain a better understanding of the transcriptomic changes at a systems level, we used weighted gene co-expression network analysis (WGCNA) (16,17). WGCNA uses transcriptomic data to identify biologically meaningful gene clusters known as co-expression modules. Co-expression modules can facilitate the finding of hub genes that are key drivers of module function and may correspond to biological pathways (18).

Data from the weeks 3 and 6 time points were used in the WGCNA analysis. The day 1 time point was not used as the large differences in developmental gene expression between day 1 and week 3 created physiologically implausible modules. The top-most variable genes (see Methods) were used as WGCNA input. Topological overlap was used for clustering, resulting in 16 modules, as can be seen from the color-band underneath the cluster tree (Fig. 2A). Modules were arbitrarily assigned colors with sizes ranging from 90 (darkgray) to gray (1604). The gray module consisted of genes that do not group into any specific module.

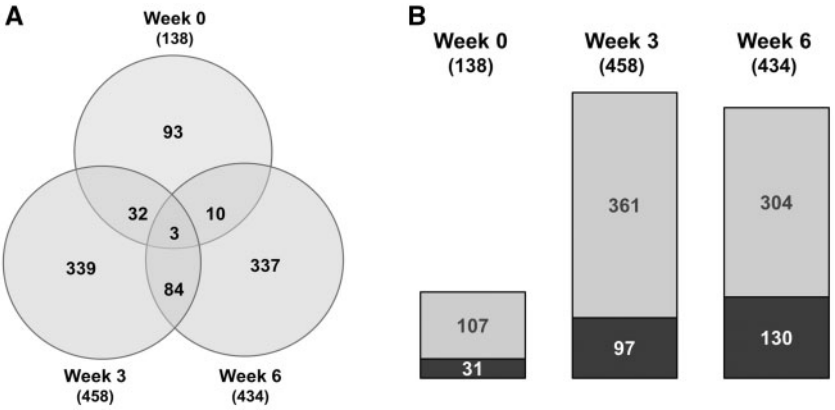

Figure 1. ATXN2-Q127 mouse cerebellar gene expression profiles at three time points. (**A**) Number of shared and specific differentially expressed genes across the three time points. (**B**) Number of differentially regulated genes in cerebella of ATXN2-Q127 mice compared with WT mice at each time point. Black (up-regulated), Gray (down-regulated).

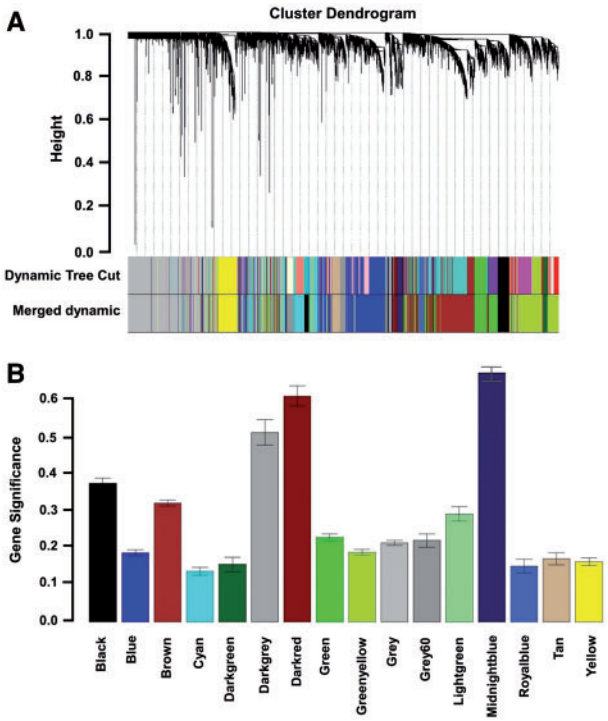

Figure 2. Gene co-expression modules. (**A**) Identification of cerebellar gene co-expression modules in ATXN2-Q127 mice with age-matched controls. Branches of the cluster dendrogram gave rise to 16 color-coded modules when modules with 10% similarity were merged. (**B**) Gene significance per module as determined by enrichment for genes with high differential expression between ATXN2-Q127 and controls. The black, darkgray, darkred and midnightblue were the only significant modules ($P < 0.05$).

Identification of modules associated with mutant polyQ-expanded ATXN2

To identify relevant modules associated with SCA2 pathology, we assessed the relationship between *ATXN2* mutation status and the module eigengene, a weighted summary of the gene expression module (19). We identified four modules, black ($r = 0.48$, $P = 6.7e{-3}$), darkgray ($r = 0.67$, $P = 1.5e{-7}$), darkred ($r = 0.79$, $P = 2.5e{-11}$) and midnight blue ($r = 0.89$, $P = 2.2e{-16}$) that showed significant enrichment for genes with differential expression between ATXN2^{Q127} and WT mice (Fig. 2). Figure 3 visualizes the connectivity patterns and hub genes (Table 1) of the relevant modules. Hub genes are identified per module using WGCNA's intramodular connectivity score, a measure of the cumulative connectivity a gene has with all other genes in a given module.

The black module consisted of 376 genes loosely correlated with SCA2 pathology. GO analysis revealed that the module was enriched with genes identified as regulators of small GTPase-mediated signal transduction ($P = 1.8e{-3}$), mRNA transport ($P = 5.2e{-3}$) and phosphorylation ($P = 5.4e{-3}$). KEGG pathway analysis showed this module to be enriched for axon guidance ($P = 4.8e{-3}$).

The darkgray module contained 90 genes including multiple PC markers as defined by Rong *et al.* (14), including *Calb1, Car8, Casq2, Fgf7, Gng13, Kitl, Pcp4, Stk17b, Sycp1* and *Trpc3*. GO analysis revealed enrichment of terms related to ER-nuclear signaling ($P = 3.5e{-3}$), regulation of apoptosis ($P = 1.3e{-2}$) and positive regulation of cell differentiation ($P = 2.4e{-2}$). Interestingly, many of the PC marker genes were also highly connected hub genes, such as *Calb1*, *Stk17b* and *Pcp4*.

The darkred module had 107 genes including multiple PC markers (*Garnl3, Homer3, lcmt, Itpka, Pcp2* and *Slc1a6*). GO analysis revealed genes enriched with terms related to regulation of small GTPase-mediated signal transduction ($P = 5.2e{-5}$) and intracellular signaling cascade ($P = 4.2e{-4}$).

The midnightblue module had the highest correlation with disease status as determined by the gene significance (GS) measure. It contained 159 genes, including PC markers *Atp2a3, Cacna1g, Dner, Doc2b, Grid2, Inpp5a* and *Itpr1*. Interesting enriched GO terms included metal ion transport ($P = 5.6e{-5}$), cerebellar PC layer development ($P = 4.1e{-3}$) and synaptic transmission ($P = 8.2e{-3}$). KEGG pathway analysis revealed the module to be related to long-term depression ($P = 2.5e{-4}$), phosphatidylinositol signaling system ($P = 2.9e{-3}$) and the calcium signaling pathway ($P = 392e{-3}$), all pathways well known to be crucial for PC functioning.

Validation of key DEGs

We validated the relative expression levels of hub genes from the co-expression network analysis using quantitative reverse transcriptase polymerase chain reaction (RT-PCR) (Fig. 4). We found 13 of the 15 genes analyzed were significantly differentially expressed in the cerebella of ATXN2^{Q127} mice compared with WT

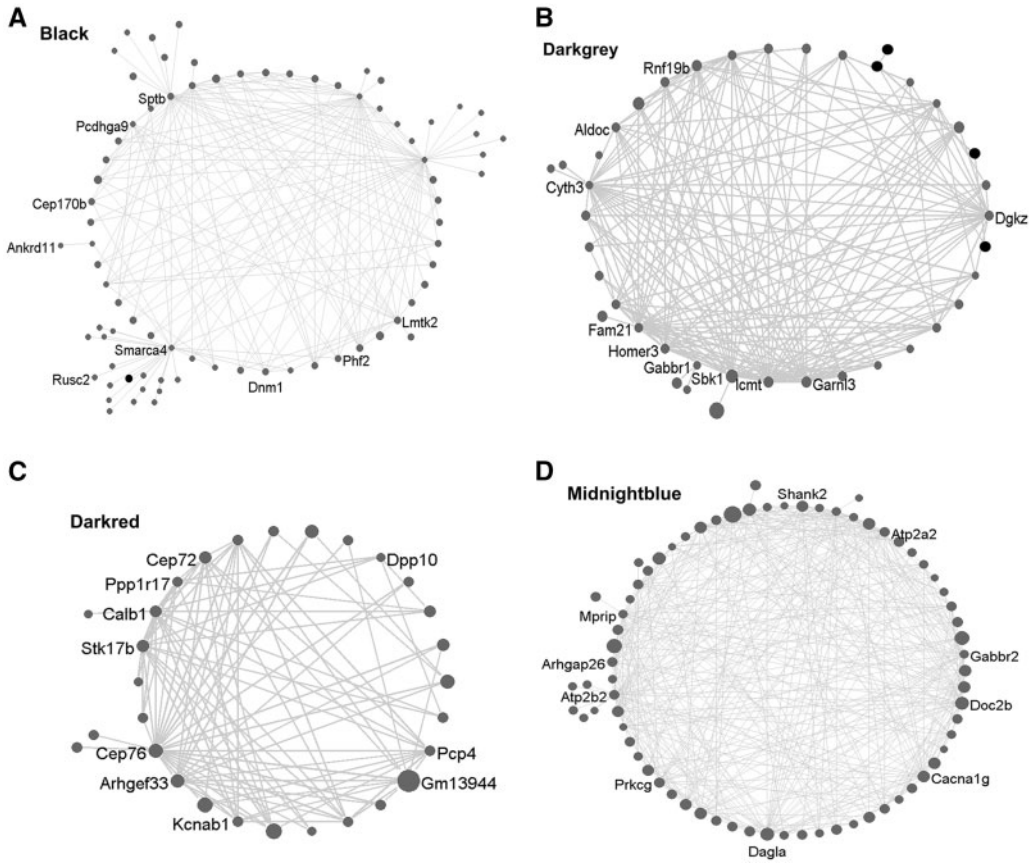

Figure 3. Co-expression networks of relevant modules. Network representation of the (**A**) black, (**B**) darkgray, (**C**) darkred and (**D**) midnightblue modules. Visual representation generated using VisANT (53). Given TOM cut-offs, not all genes corresponding to each module are represented.

Table 1. Top 10 hub genes as ranked by intramodule connectivity for each of the gene significant modules

Black	Darkgray	Darkred	Midnightblue
Smarca4	*Cep76*	*Cyth3*	*Gabbr2*
Rusc2	*Calb1*	*Dgkz*	*Dagla*
Pcdhga9	*Stk17b*	*Gabbr1*	*Doc2b*
Ankrd11	*Pcp4*	*Sbk1*	*Atp2a2*
Lmtk2	*Dpp10*	*Fam21*	*Prkcg*
Sptb	*Kcnab1*	*Icmt*	*Atp2b2*
Dnm1	*Ppp1r17*	*Rnf19b*	*Mprip*
Cep170b	*Cep72*	*Garnl3*	*Cacna1g*
Phf2	*Gm13944*	*Aldoc*	*Arhgap26*
Agap1	*Arhgef33*	*Homer3*	*Shank2*

littermates. Validated hub genes include *Sptb* from the black module, *Gabbr2* from the midnightblue module, *Cep76, Calb1* and *Pcp4* from the darkgray module and *Gabbr1, Fam21, Dgkz* and *Aldoc* from the darkred module. *Casp3* was also validated as significantly up-regulated in mice age 3 weeks.

MicroRNAs

Several links between microRNA (miRNA) regulation and polyglutamine repeat associated ataxias are known (20,21). To identify alterations in miRNA expression associated with SCA2, cerebellar samples from mice 3 weeks of age and age-matched controls were used to isolate total RNAs. Small RNA libraries were generated from four biological replicates from each group and subsequently sequenced on an Illumina HiSeq platform. An average of 29.6 million reads was generated from the eight libraries, ranging from 23.1 to 36.3 million. Out of the 297 million reads, 135 were able to be mapped to the mouse genome (mm10). Differential expression analysis was performed and identified 16 annotated miRNA and 4 snoRNAs with fold changes greater than 1.5 ($P < 0.01$). With the exception of the snoRNA *Gm24895*, all transcripts were down-regulated in cerebella of ATXN2^{Q127} mice (Table 2).

To gain a better understanding of the role of the differentially expressed miRNAs in SCA2 pathogenesis, we identified all known and predicted miRNA binding targets using Tarbase and TargetScan, respectively (22–24). The known and predicted binding targets were then intersected with the significantly up-regulated genes from the 3 week mRNA time point. The only known binding target found in Tarbase was *Trim59*, a target of miR-499. An additional 20 binding targets were predicted using TargetScan (Supplementary Material, Table S4).

Atxn2$^{-/-}$ mice have few cerebellar DEGs

Atxn2 deficient mice (*Atxn2*$^{-/-}$) are viable and have only slight phenotypic changes compared with WT littermates (7). However, it is unknown if the non-essential role of ataxin-2 in mice is due to the presence of orthologs or redundant mechanisms. To further investigate the role of *Atxn2*, we analyzed gene expression using RNA sequencing of cerebellar tissues of *Atxn2*$^{-/-}$ and age matched WT mice. Cerebella from 1 day and

60-day-old WT, heterozygous ($Atxn2^{+/-}$) and $Atxn2^{-/-}$ mice were collected, each with four biological replicates. RNA libraries were generated from each group and subsequently sequenced on an Illumina HiSeq platform.

We identified 46 differentially expressed cerebellar genes (fold change $\geq$1.5 or ≤ -1.5, P-value <0.01) between $Atxn2^{-/-}$ and age matched WT mice at 1 day and 11 genes at 60 days (Supplementary Material, Table S5). Only two genes were differentially expressed at both time points (*Ubc*, *Gm8730*). Of the DEGs, 16 were up-regulated and 30 were down-regulated at age 1 day and five were up-regulated and six down-regulated in mice 60 days of age.

No pathway overlap between $Atxn2^{-/-}$ and $ATXN2^{Q127}$ mice

To find overlapping pathways between $Atxn2^{-/-}$ and $ATXN2^{Q127}$ mice, we compared the overlap among DEG lists at the 60 day and 6 week time points, respectively (Fig. 5). The remarkably few number of significantly changed cerebellar genes between $Atxn2^{-/-}$ and WT mice, in contrast to the large number of differentially expressed genes between $ATXN2^{Q127}$ and WT mice is consistent with the gain-of-function model for the expanded polyglutamine disease.

PC firing rates in the acute cerebellar slice in $Atxn2^{-/-}$ mice

After considering the lack of phenotypic and transcriptomic similarities between the $Atxn2^{-/-}$ and $ATXN2^{Q127}$ mice, we elected to investigate electrophysiological behavior of $Atxn2^{-/-}$ PCs. This allowed the examination of the effect of *Atxn2* knockout on the neurophysiological phenotype using previously established methods (3,5). We utilized non-invasive extracellular recording techniques to measure the intrinsic PC firing rate in acute cerebellar slices at ages 4, 12 and 24 weeks. The average mean firing frequency over populations of PCs is shown in Figure 6 using population distributions. To generate the distribution, the mean firing frequency was calculated over 2 min time periods for multiple PCs and plotted for each age. The mean firing frequency is indicated for each age in Figure 6. In contrast to $ATXN2^{Q127}$ animals that show a progressive slowing of PC firing beginning at age 8 weeks, the firing frequency remained normal in $Atxn2^{-/-}$ mice.

Discussion

We performed RNA sequence analysis in an SCA2 mouse model that targets expression of the mutant polyQ-expanded ATXN2 to PCs. Our use of multiple time points and differential expression analysis showed that genes were differentially expressed as early as 1 day, with an increasing number of genes and progressively greater fold-changes at later time points. Furthermore, 16 miRNAs and 4 snoRNAs were differentially expressed as early as 3 weeks. These observations were all performed with stringent cut-offs for fold-change and significance levels for multiple comparisons.

Subsequent analysis of the DEGs using WGCNA allowed us to identify four gene modules related to disease progression. Investigation of these modules revealed novel hub genes and pathways that are likely biologically relevant to disease initiation and progression.

Comparison of the $ATXN2^{Q127}$ and $Atxn2^{-/-}$ expression datasets showed negligible overlap. Additionally, PC firing in the acute slice in the knock-out model was unchanged, in contrast to the transgenic model, in which the intrinsic firing frequency progressively slows with age (3). Taken together, these data give insight into SCA2 disease progression and are consistent with a gain-of-toxic-function associated with *ATXN2* mutation. Furthermore these data support ongoing research on the development of SCA2 therapeutics that lower *ATXN2* expression targeting both WT and mutant alleles.

Transcriptomic comparison

Several studies have examined changes in mRNA steady-state levels in SCA mouse models. Most of these used expression arrays (25–27), but a recent analysis of an SCA1 model employed RNA-seq and analysis by WGCNA (28). Transcription dysregulation commonly seen in polyglutamine disorders and comparison of gene expression among the polyglutamine diseases has revealed many commonly occurring changes (27,29). We also find similarities between published polyglutamine expression profiles and our SCA2 profile. Everet *et al.* determined gene expression changes in SCA3 cell models (30). While not a perfect comparison, non-cerebellar genes and pathways were revealed. Of note, both studies demonstrated changes to extra-cellular related molecules such as *Timp1* and *Timp2*. Our full differential expression analysis, discussed below, showed large changes in genes associated with the ECM occurring as early as day 1. This overlap suggests disruption of processes involved with the ECM such as cellular adhesion. Similarly we find high overlap with laser-capture PC expression profiles from Huntington disease and SCA7 mice (27). Many PC markers were common to both sets including *Calb1, Pcp4, Itpr1, Slc1a6* and *Pcp2*. Other overlapping genes that were also differentially expressed in SCA1, SCA3, SCA7 or DRPLA included *Grid2*, *Aloc, Fam107b, Dagla, Rgs8, Nptx1* and *Plcb3*. Furthermore, many movement disorders are associated with the dysfunction of PGC-1α, a master regulator of mitochondrial biogenesis. While not a polyglutamine expansion disease, Lucas *et al.* showed evidence of PC loss and an ataxia phenotype in a PGC-1α deficient mouse model (31). Microarray analysis of the PCGA-1a deficient mouse model found novel genes associated with the deletion, however, no overlap was found between these transcripts and the SCA2 profile, suggesting different roles in neurodegeneration.

Comparison to similar studies on SCA1

Although the disease models mentioned above provide an insight into shared transcriptome changes in neurodegeneration, the recently published SCA1 dataset is most relevant to our study as it uses a comparable animal model and similar technology for analysis (28). Ingram *et al.* used RNA sequencing of SCA1 mouse cerebellar tissues and subsequent WGCNA analysis to identify two modules related to SCA1 pathology, Magenta and Lt. Yellow. We found no significant overlap with the SCA1 Lt. Yellow module but three of our SCA2-related modules (darkgray, darkred and midnightblue) had significant overlap with the SCA1 magenta module. There were 33 genes of the SCA1 magenta module that overlapped with the SCA2 darkgray module ($P < 0.001$), 34 with the darkred module ($P < 0.001$) and 51 with the midnightblue module ($P < 0.001$) (Supplemental Material, Table S6). Using the top 100 connected genes of the SCA1 magenta module, we found that 92 are also in the overlapping SCA2 modules including

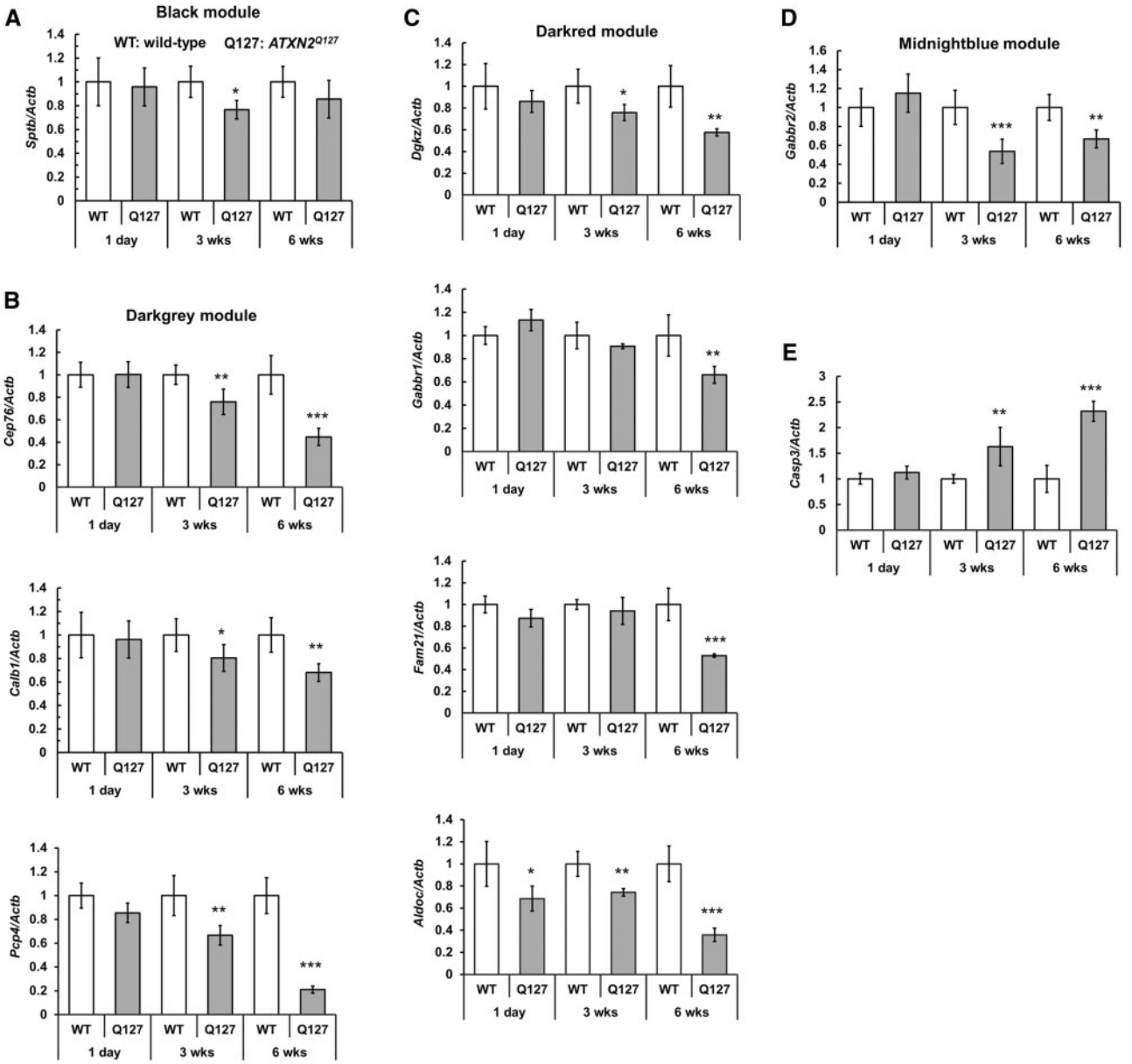

Figure 4. Validation of key genes. Validation of key transcript changes in $ATXN2^{Q127}$ transgenic mice. Cerebellar transcripts with significantly different expressions in $ATXN2^{Q127}$ mice compared with WT littermates were verified using quantitative RT-PCR. Validated genes include *Sptb* (Black module), *Cep76*, *Calb1* and *Pcp4* (darkgray); *Dgkz*, *Gabbr1*, *Fam21* and *Aldoc* (darkred); *Gabbr2* (midnightblue), and *Casp3 (Midnightblue)*. Values shown are means and SD; $n = 6$ mice.

multiple PC marker genes. Furthermore, we found that genes identified as highly interconnected or hub genes in the SCA1 magenta module were also found to be highly interconnected in the SCA2 modules including *Fam21*, *Gabbr1* and *Homer3* from the magenta/darkred module overlap and *Rgs8* and *Lcmt* from the magenta/midnightblue overlap. To identify why one SCA1 module had significant overlap with three SCA2 modules, we re-analyzed our SCA2 data with increased merge cut-height and soft-threshold power. The re-analysis resulted in a module (purple) with a larger overlap genes (Supplementary Material, Table S6), suggesting module differences are a result of WGCNA parameters and filtering choices. The SCA1 study also revealed a likely PC protective gene, *Cck*. We also detected significant differential expression of this gene and the associated receptors (*Cckar*, *Cckbr*) in our SCA2 model.

Temporal mRNA changes

Changes in expression as early as day 1. The use of multiple time points allowed us to identify early changes and trends associated with disease pathology. We observed that the presence of an expanded ATXN2 polyQ repeat resulted in altered gene expression as early as day 1. While a smaller number of genes were altered compared with the later time points, a portion of these genes were associated with terms suggesting a disruption of normal development. For instance, up-regulated genes are associated with histone acetylation and chromatin remodeling while down-regulated genes are associated with cell adhesion and extracellular matrix terms. It is unknown whether the disruption caused early morphological differences or delayed development. Many of the genes associated with cell growth and development, however, remained down-regulated in mice

Table 2. Differentially expressed miRNA and snoRNA at 3 weeks of age

Gene name	Gene biotype	Location	Fold change	P-value
snord115	snoRNA	chr7:59389819–59389898	−23.858195	<0.001
snord115	snoRNA	chr7:59424923–59425002	−15.602832	<0.001
snord115	snoRNA	chr7:59353282–59353361	−9.9424817	<0.001
snord115	snoRNA	chr7:59436148–59436227	−3.7960027	<0.001
snord115	snoRNA	chr7:59423054–59423133	−3.3968088	<0.001
Mir199b	miRNA	chr2:32318459–32318569	−2.4620806	<0.001
Mir203	miRNA	chr12:112130879–112130955	−2.6289378	<0.001
Mir499	miRNA	chr2:155622879–155622958	−2.1579763	<0.001
Mir1197	miRNA	chr12:109712316–109712436	−2.5935263	0.00254961
Mir142	miRNA	chr11:87756863–87756927	−2.6020848	0.002499857
Mir1193	miRNA	chr12:109715670–109715791	−2.1320688	0.007377873
snord116	snoRNA	chr7:59681054–59681148	−2.5926653	0.002554669
Mir144	miRNA	chr11:78073004–78073070	−2.6183301	0.002408074
Mir653	miRNA	chr6:3721300–3721385	−2.4714334	0.003377277
Mir544	miRNA	chr12:109729324–109729402	−2.1655448	0.006830543
Mir208a	miRNA	chr14:54949059–54949142	−2.0384873	0.009151929
Gm24895	snoRNA	chr12:109646128–109646202	−0.4719824	0.33730097
Mir669l	miRNA	chr2:10468970–10469068	−1.9343033	0.011633134
Gm22620	snoRNA	chr9:15315188–15315321	−1.8507692	0.014100379
Mir133b	miRNA	chr1:20682768–20682887	−1.9097873	0.012308713
Mir214	miRNA	chr1:162223367–162223477	−2.0388675	0.009143922
Mir3059	miRNA	chr10:101772691–101772772	−2.3094863	0.004903585
Mir483	miRNA	chr7:142654923–142654996	−1.8474739	0.014207775
Mir708	miRNA	chr7:96249423–96249532	−2.2037934	0.006254701

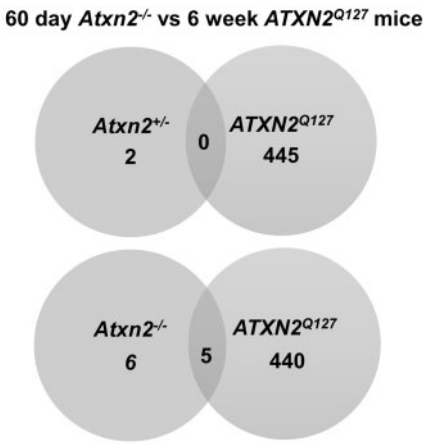

Figure 5. Comparison of differentially expressed genes between mouse models. Venn diagrams of differentially expressed genes (Het = $ATXN^{+/-}$, KO = $ATXN2^{-/-}$ and TG = $ATXN2^{Q127}$) at 60 day/6 week time points.

3 weeks of age. Of note, detailed morphology and physiology of transgenic cerebella did not show any changes prior to 6 weeks of age.

Changes in pathways controlling calcium and glutamatergic synapses. In a recent review of cellular and circuit mechanisms underlying spinocerebellar ataxias, we showed that disrupted calcium homeostasis caused by impaired metabotropic glutamate receptor signaling is a common PC pathophysiological mechanism in SCAs (32). Irregularities in calcium signaling have been associated with multiple neurodegenerative diseases including SCA2 (33–36), and multiple knock-out mouse studies have shown that genetic deficiencies in the glutamate receptor pathway lead to ataxia (32). Therefore, we sought to determine if pathways controlling calcium and glutamatergic signaling were modified in an age-dependent manner. We observed 1 calcium ion binding genes down-regulated in 1-day-old mice, and 23 down-regulated calcium signaling genes at in 3 week old mice that persisted to 6 weeks of age. KEGG pathway analysis supported this observation, showing that calcium signaling was not a significant pathway in 1 d old mice but was significantly altered in both the 3 and 6 week old mouse groups (Supplemental material, Table S2). Similarly, we observed a set of significantly changed genes controlling glutamatergic synapses according to KEGG pathway analysis that were not changed in 1 day old mice but significantly enriched at 3 weeks and increasingly at 6 weeks *(Plcb3, Gnao1, Grik1, Homer3, Slc1a6, Gng13, Gria3, Prkcg, Shank1, Gng4, Shank2, Itpr1*). Mutations in two of these genes, *Prkcg* and *Itpr1*, are the cause of SCA14 and SCA15, respectively (37,38). These findings are consistent with the hypothesis that dysregulated calcium pathway signaling and metabotropic glutamate receptor signaling contributes to ataxia through elevated calcium leading to hyperexcitability and reduced PC firing frequency (32).

Apoptosis by week 6. Examining the widespread expression changes occurring by week 6, we noticed a subset of up-regulated genes. These genes were largely associated with regulation and activation of apoptosis including *Casp3, Bid, Hrk, Btg2, Hspa1, Hgf, Ntf3* and *Timp1*. With the accompanying down-regulation of many PC markers, we suggest that PC degeneration begins to occur as early as 6 weeks, after notable dysregulation of genes associated with calcium signaling changes.

Knock-out changes

Previous studies demonstrated that SCA2 pathogenesis was likely caused by gain-of-toxic-function due to the expanded polyQ repeat in ATXN2 (39). *Atxn2*$^{-/-}$ mice had no CNS abnormalities or neurodegeneration and easily became obese but also had abnormal fear conditioning associated with altered long-

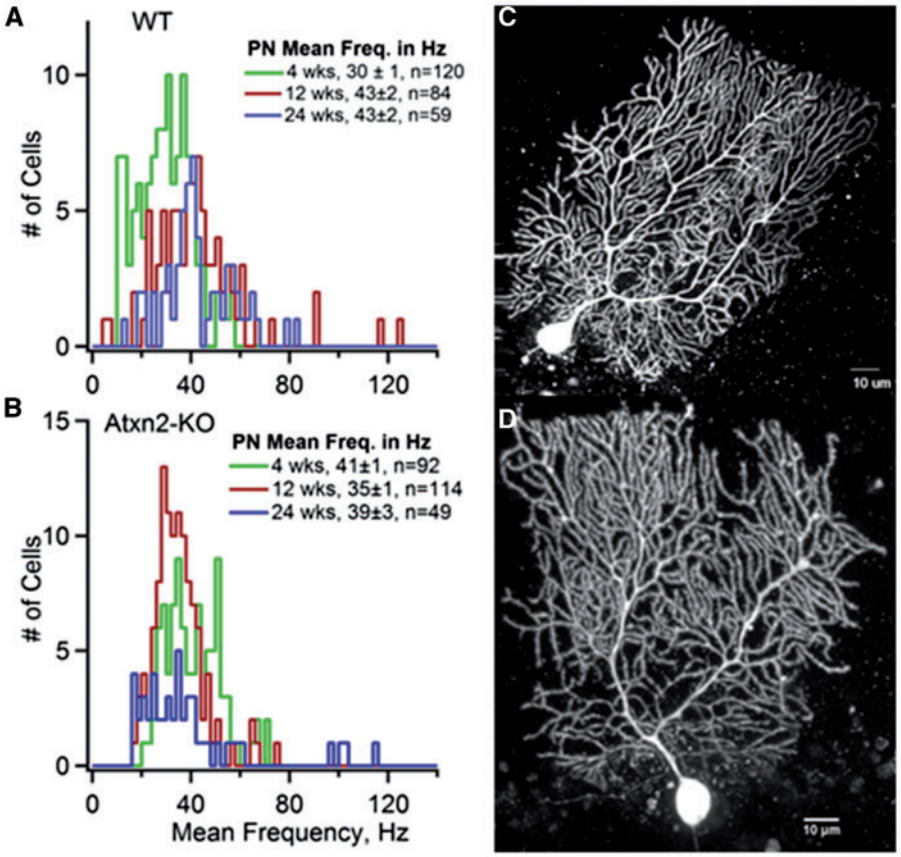

Figure 6. Knockout of the *Atxn2* gene in mice did not change Purkinje cell firing in the acute cerebellar slice. Purkinje cell firing frequency distribution plots determined by extracellular recordings in acute cerebellar slices from WT (**A**) and *Atxn2*-knockout (KO) (**B**) mice ages 4, 12 and 24 weeks. Alexa Fluor 488 filled Purkinje Neuron in WT (**C**) and $ATXN2^{-/-}$ (**D**) in 24 weeks old mice.

term potentiation in the amygdala (8). Additionally, investigations on SCA6 and SCA7 showed no evidence for contribution to neurodegeneration by loss of function attributed to CAG expansion mutation in the causative disease genes (*Cacna1a* and *Atxn7*, respectively) (35,40). However, the deletion of *ATXN1* enhanced SCA1 pathogenesis (41).

We used deep-RNA sequencing to confirm suspected minimal transcriptomic changes associated with the lack of CNS abnormalities previously observed in $Atxn2^{-/-}$ mice. Disease progression by 6 weeks caused large transcriptional changes in the $ATXN2^{Q127}$ mouse with over 400 genes differentially expressed when compared with WT. In contrast, relatively small changes were seen in the $Atxn2^{-/-}$ mouse model with only 11 genes differentially expressed when compared with WT at an age, 60 days, when the transgenic mouse shows significant disease. Comparing the overlap between $Atxn2^{-/-}$ and $ATXN2^{Q127}$ transcriptomes at the later time point showed that five out of the 11 $Atxn2^{-/-}$ DEGs were shared with $ATXN2^{Q127}$. While this overlap was significant, the small number of expression changes argues strongly that loss-of-function is not a significant part of disease pathology. In addition, the day 1 comparison had only three overlapping genes (Supplementary Material, Table S5). The lack of overlap is consistent with a gain-of-function in SCA2 mice. In contrast to transcriptome analyses of SCA1 mice indicating gain-of-function with partial loss of function (41), we could find little evidence for partial loss-of-function in our SCA2 mice. These conclusions based on transcriptome analyses were also supported by the lack of PC firing changes in the acute cerebellar slice in knockout animals. Whereas $ATXN2^{Q127}$ animals show a progressive decline in spontaneous PC firing beginning at 8 weeks of age, PCs in $Atxn2^{-/-}$ mice retained a normal firing rate even as late as 24 weeks of age.

Weighted gene co-expression network analysis

WGCNA is a technique used to identify highly correlated gene modules which can be related to external factors such as disease status. We applied this unsupervised, hypothesis-free method to construct co-expression networks in polyQ expanded SCA2, revealing pathologically relevant gene modules. This approach has been used successfully for the study of multiple neurodegenerative diseases, helping to elucidate disease pathways and associated genes (42–45). In SCA2, little is known about gene expression changes that precede electrophysiological and motor phenotypes in SCA2 disease progression. The use of a hypothesis-free approach allowed us to increase the current knowledge of expanded polyglutamine pathology in SCA2 and provide new avenues for future research.

Modules

We identified four modules correlated with disease status that can be summed into known pathological associations with SCA2 including GTPase mediated signaling, calcium signaling and cell death. Interestingly, the largest of these, the black module, did not

contain any PC markers. It contained multiple genes associated with regulation of small GTPase signal transduction (*Plekhg3, Smap2, Bcr, Sgsm1, Tbc1d9, Tiam1, Prex1, Trio, Agap1, Tbc1d22b, Rapgef1, Arhgef11*), synaptogenesis (*App, Nrxn2, Dlg4*) and axon guidance (*Ablim1, Ablim2, Sema4g, Unc5a, Plxnb3, Sema4b, Sema4d, Sema3a*). This module provides an insight into the dysregulation of neurodegenerative cell morphology. The darkred module is similarly associated with regulation of GTPase-mediated signal transduction (*Garnl3, Agfg2, Rapgef6, Iqgap2, Dgkz, Icmt, Cyth3, Psd2*). However, it was not found to be enriched for any other GO term or KEGG pathways. The darkgray module is enriched for genes associated with programmed cell death (*Trp53, Stil, Clu, Stk17b, Eif2ak3, Kitl, Acvr1c*). It provides additional information on the early apoptotic cycle in the cerebellum. Of note, pathway analysis of this module showed an overlap with pathways associated with cancer due to the genes *TRP53, CCND1, FGF7* and *ACVR1C*. Also, three of the top four genes ranked by intermodular connectivity, or hub genes, are known PC markers *Calb1, Stk17b* and *Pcp4* providing evidence that further analysis of this module may provide novel PC markers. Lastly, the midnightblue module is significantly associated with calcium signaling (*Atp2b2, Plcb3, Atp2a2, Atp2a3, Cacna1g, Grm1, Itpr1*) and PC layer development (*Atp2b2, Lhx5, Klhl1*). Further investigation into this module could elucidate early transcriptional changes in PCs. This module also had overlap with an Alzheimer's disease pathways. Complete GO term categories and associated genes can be found in the Supplementary Material, Table S6.

microRNAs in SCA2

Finally, the identification of early transcriptional changes in miRNAs presents opportunities for further investigation into disease pathogenesis. MiRNAs and snoRNAs have important roles in many neurodegenerative diseases, including Parkinson disease, amyotrophic later sclerosis and Alzheimer's disease (21,46,47). Our results of 3-week-old mice show changes in 16 annotated miRNAs and 4 snoRNAs. Further analysis of the 16 miRNA gene binding targets found 1 known binding target and 20 predicted targets. The only known binding interaction was between miR-499 and *Trim59*. *Trim59* has been implicated in multiple processes but has recently been shown to be a key regulator in cancer cell proliferation by upregulating cell cycle-related proteins and a negative regulator of KF-kβ signaling (48,49). We also observed that the week 3 GO analysis showed significant dysregulation of other genes associated with negative regulation of NF-kappaB signaling (*Olfm4, Trim59, Nfkbid* and *Tnip1*). The downregulation of this pathway is a constant with a response to cellular stress and apoptosis. An intersection of the 21 potential binding targets with the WGCNA analysis showed that only *Adcyap1* is in a gene-significant module, midnightblue. No other common pathways or SCA related genes were identified suggesting further analysis of the role of miRNA in SCA2 is needed.

The top differentially expressed snoRNA, *Snord115*, which has an average of over >10-fold decrease when compared with WT. Since *Snord115* is a gene cluster containing at least 130 copies in mouse, it is possible that the difference in expression is due to sequencing alignment error. However, RT-PCR analysis validated the decrease when compared with WT, although the magnitude of change is smaller with only a 40% decrease (Supplementary Material, Fig. S1). Additionally, previous studies have demonstrated that increased expression of Snord115 correlates with increased calcium ion response to GPCR mediated signaling (50). Considering the notable changes to genes associated with calcium signally at 3 weeks of age, it is plausible that the large decrease of this snoRNA in ATXN2^{Q127} is in response to an early imbalance in calcium signaling.

In contrast to microRNA studies in SCA1 pathogenesis, the majority of SCA2 microRNA's are down-regulated. A miRNA expression study in SCA1 transgenic mice identified a larger number of up-regulated genes than down-regulated with only miR-203 being shared with the SCA2 dataset (47). Using microarray analysis of cerebellar and cortical RNA samples from SCA1 patients, Persengiev *et al.* showed that the majority of miRNA changes were up-regulated when compared with healthy individuals with few being down-regulated (51). Of the down-regulated genes, miR-144 is present in both SCA1 and SCA2 datasets. MiR-144 has been shown to directly bind *ATXN1* and repress expression. While no direct interaction between ATXN2 and miR-144 has been shown, miRNA prediction suggests mir-144 will bind and downregulate the *ATXN2* gene (52). Downregulation in both SCA1 and SCA2 suggests that mir-144 dysregulation is not directly linked to mutant gene expression but results from a shared functional pathway in neurodegeneration.

Materials and Methods

Animals

Transgenic and knock-out mouse line generation and characterization have been previously described (3,7). Mouse line background slightly differed between transgenic mouse lines with the 3 and 6 week animals being N4F1 in a B6D2 mixed hybrid background. The 1 day old Q127 are N5F0 B6D2 mixed hybrid background. The 1 and 60 day SCA2 KO mice are 50/50 C57B6/Fvb129 mice.

RNA sequencing and analysis

Total RNA was isolated using miRNeasy Mini Kit (Qiagen Inc., USA) according to the manufacturer's protocol. RNA quality was determined using the Bioanalyzer2100 Pico Chip (Agilent). Samples with an RNA integrity number (RIN) >8 were used for library preparation using Illumina TrueSeq Stranded Total RNA Sample Prep with Ribo-Zero rRNA Removal Kit for mouse. Single-end 50-bp reads were generated on a Hiseq 2000 sequencing machine at the University of Utah Microarray and Genomic Analysis Shared Resource using Illumina Version 4 flow cells. Reads were then aligned to the mouse reference genome (mm10) by Novoalign (http://www.novocraft.com; date last accessed May 22, 2017). Quality of RNA sequencing was good with an average of 22 million reads for ATXN2^{Q127}. Ninety eight percent of the reads were aligned to the reference mouse genome. After read alignment, differentially expressed genes were identified using the DRDS application (version 1.3.0) in the USeq software package (http://useq.sourceforge.net/; date last accessed May 22, 2017).

Co-expression network

RNA-seq data from the weeks 3 and 6 time-points were first filtered by FPKM (≥1.0 in 90% of samples) to reduce noise. Further filtering on the coefficient of variation (≥0.15) was used to get the most variable genes, resulting in 7694 transcripts. The unsigned WGCNA was conducted as previously described using the R package WGCNA (PMID 19114008). Briefly, a similarity matrix was constructed using the Pearson correlation coefficients created between the FPKM normalized expression levels of the input transcripts. By raising the absolute value of the Pearson

correlation coefficients to a power of 14, we were able to get a scale-free topology index above 0.9, achieving a network with few, large correlations at the expense of lowly correlated transcripts. This allows for the fewer, highly connected and biologically relevant hub genes. An adjacency network was then created using topological overlap measure (TOM), a measure of neighborhood connectivity. To create modules, the adjacency network was converted into a dissimilarity measure (1 – TOM) and clustered using flashClust, a hierarchical clustering function. Cluster branches were cut to identify modules. Module size was set to a minimum of 50 transcripts and modules with a 10% similarity were merged using dynamic tree cutting, resulting in 16 modules. To identify significant modules, GS was calculated as the absolute value of the correlation between gene expression and transgenic status. Overall significance for each module was calculated by averaging all GS within each module. Statistical significance was determined using the correlation *t*-test *P*-value.

RNA expression analyses by quantitative RT-PCR

Mice were deeply anesthetized with isoflurane. Mouse cerebella were removed and immediately submerged in liquid nitrogen. Tissues were kept at −80 °C until the time of processing. Total RNA was extracted from mouse cerebella and harvested cells using RNAeasy mini-kit (Qiagen Inc., USA) according to the manufacturer's protocol. DNAse I treated RNAs were used to synthesize cDNA using ProtoScript cDNA synthesis kit (New England Biolabs Inc., USA). Quantitative RT-PCR was performed in QuantStudio 12K (Life Technologies, Inc., USA) with the Power SYBR Green PCRMaster Mix (Applied Biosystems Inc, USA). PCR reaction mixtures contained SYBR Green PCRMaster mix, synthesized cDNA and 0.5 pmol primers, and PCR amplification was carried out for 45 cycles: denaturation at 95 °C for 10 s, annealing at 60 °C for 10 s and extension at 72 °C for 40 s. The threshold cycle for each sample was chosen from the linear range and converted to a starting quantity by interpolation from a standard curve run on the same plate for each set of primers. All gene expression levels were normalized to the Actin mRNA levels. Primer pairs designed for qPCR are given as forward and reverse, respectively, and listed in Supplementary Material, Table S7. The miRNA cDNA was transcribed by using TaqMan MicroRNA Reverse transcription kit (Cat no. 436596, Life Technologies, Inc., USA). The level of miRNA was analyzed by qPCR using the microRNA203 Assay (ID #001196) and U6 snRNA Assay (ID #00973) for normalization.

Functional enrichment analysis

Gene ontology and pathway-enrichment analysis (KEGG) was conducted using the functional annotation tool DAVID (https://david.ncifcrf.gov/; date last accessed April 18, 2017). Enriched ontological terms and pathways with *P* values <0.05 were selected.

MircoRNA

Cerebellar extract from mice 3 weeks of age with 4 biological replicates and age-matches WT controls were used for microRNA library construction. The construction of Small RNA sequencing libraries was performed using the Illumina TruSeq Small RNA Sample Prep Kit (RS-200-0012, RS-200-0024). Most mature miRNAs have a 5'-phosphate and a 3'-hydroxyl as a result of the cellular pathway that creates them. The adapters are designed to specifically ligate to RNA molecules containing these terminal modifications. Briefly, total RNA (1 μg) was denatured and 3' and 5' RNA adapters were sequentially ligated to appropriately modified ends of RNA molecules. Adapter-ligated RNA was reverse transcribed using a RNA primer complimentary to the 3'-adapter sequence and Superscript II Reverse Transcriptase (Invitrogen cat#18064-014). Adapter sequences were extended and index tags are added to the reverse transcribed cDNA by PCR (11 cycles). The PCR-amplified library is resolved on a 6% 25 Novex TBE PAGE gel (Invitrogen cat# EC6265BOX) and a gel fragment representing the size range of adapter-modified small RNA cDNA was excised from the gel. Small RNA library molecules were eluted by soaking the crushed gel fragment overnight in ultra-pure water at room temperature. Gel debris was removed from the eluate by centrifugal filtration of the sample across a 5-μm filter. The concentration of the small RNA library was measured using the Invitrogen Qubit dsDNA HS Assay (Q32851) and an aliquot of the library was resolved on an Agilent 2200 Tape Station using a High Sensitivity D1K (cat# 5067-5363 and 5067-5364) assay to define the size distribution of the sequencing library. Libraries were adjusted to a concentration of ∼5 nM and quantitative PCR was performed using the KapaBiosystems Kapa Library Quant Kit (cat# KK4824) to calculate the molarity of adapter ligated library molecules. The concentration was further adjusted following qPCR to prepare the library for Illumina sequence analysis.

Electrophysiology

Parasagittal cerebellar slices were made as described earlier in Hansen *et al.* (3). In brief, age-matched WT and ATXN2-KO mice were anesthetized using isoflurane and sacrificed in accordance with the protocol approved by the University of California Los Angeles Institutional Animal Care and Use Committee. The cerebellum was quickly dissected and placed in ice-cold extracellular solution (119 mM NaCl, 26 mM $NaHCO_3$, 11 mM glucose, 2.5 mM KCl, 2.5 mM $CaCl_2$, 1.3 mM $MgCl_2$ and 1 mM NaH_2PO_4, pH 7.4 when gassed with 5% CO_2 and 95% O_2). Parasagittal cerebellar slices (285-μm) were prepared on a VT1000 vibratome (Leica, Germany) in ice-cold extracellular solution. Cerebellar slices were then incubated at 35 °C for 30 min and stored at room temperature until use. Temperature was set to 34.5 ± 1 °C (Model TC-344B, Warner Instruments) in the recording chamber and perfused cerebellar slices with extracellular solution at a rate of 2.8–3 ml/min. Purkinje neurons were visualized with an upright microscope (Leica) using 40× water immersion objective. Recordings were carried out with borosilicate glass electrodes (World Precision Instruments, USA) of 2–3 MΩ prepared on a P-1000 capillary puller (Sutter, USA) and filled with extracellular solution. The pipette potential was held at 0 mV and placed close to the axon hillock (soma/axon) of a PC to measure action potential-associated capacitative current transients in voltage clamp mode for 2 min and typically 50–120 PCs were measured from 3 to 6 mice per genotype with the experimenter blinded to the genotype. Currents were filtered at 4 kHz and sampled at 20 kHz using a Digidata 1440 and 700B amplifier (Axon Instruments). Spike detection was performed in pClamp 10 and further analyses were made using Microsoft Excel or Igor software package. Results are expressed as mean ± SEM and figures were made in Igor. To label, whole-cell mode was used and PCs were filled with 50–100 μM fluorescent dye Alexa 488 in the internal patch pipette solution (135 mM $KMS0_4$, 10 mM NaCl, 10 mM HEPES, 3 mM MgATP, 0.3 mM Na_2GTP) for 15–30 min and then the patch pipette was withdrawn slowly to allow resealing

of the membrane. Using 2-Photon microscope, images of the intracellular Alexa 488 filled PCs were taken at wavelength of 810 nM.

Supplementary Material

Supplementary Material is available at *HMG* online.

Acknowledgements

We would like to thank the Utah Center for High Performance Computing and the High-Throughput Genomics and Bioinformatics Analysis Shared Resource Core.

Conflict of Interest statement. The authors declare no competing financial interests. SMP is a consultant for Progenitor Life Sciences and Ataxion Therapeutics.

Funding

This work was supported by grants R01NS33123, R56NS33123 and R37NS033123 from the National Institutes of Neurological Disorders and Stroke (NINDS) to S.M.P., NINDS grant R21NS081182 to D.R.S. and S.M.P., the Noorda foundation to S.M.P., the National Library of Medicine Training Grant 5T15LM007124 to L.P., and the Richard A. Fay and Carol M. Fay Endowed Graduate Fellowship for the Department of Biomedical Informatics in Honor of Homer R. Warner, M.D., Ph.D. to L.P.

References

1. Pulst, S.-M., Nechiporuk, A., Nechiporuk, T., Gispert, S., Chen, X.-N., Lopes-Cendes, I., Pearlman, S., Starkman, S., Orozco-Diaz, G., Lunkes, A. *et al.* (1996) Moderate expansion of a normally biallelic trinucleotide repeat in spinocerebellar ataxia type 2. *Nat. Genet.*, **14**, 269–276.
2. Matilla-Dueñas, A., Ashizawa, T., Brice, A., Magri, S., McFarland, K.N., Pandolfo, M., Pulst, S.M., Riess, O., Rubinsztein, D.C., Schmidt, J. *et al.* (2014) Consensus paper: pathological mechanisms underlying neurodegeneration in spinocerebellar ataxias. *Cerebellum*, **13**, 269–302.
3. Hansen, S.T., Meera, P., Otis, T.S. and Pulst, S.M. (2013) Changes in Purkinje cell firing and gene expression precede behavioral pathology in a mouse model of SCA2. *Hum. Mol. Genet.*, **22**, 271–283.
4. Dansithong, W., Paul, S., Figueroa, K.P., Rinehart, M.D., Wiest, S., Pflieger, L.T., Scoles, D.R. and Pulst, S.M. (2015) Ataxin-2 regulates RGS8 translation in a new BAC-SCA2 transgenic mouse model. *PLoS Genet.*, **11**, e1005182.
5. Scoles, D.R., Meera, P., Schneider, M.D., Paul, S., Dansithong, W., Figueroa, K.P., Hung, G., Rigo, F., Bennett, C.F., Otis, T.S. *et al.* (2017) Antisense oligonucleotide therapy for spinocerebellar ataxia type 2. *Nature.*, **544**, 362–366.
6. Damrath, E., Heck, M.V., Gispert, S., Azizov, M., Nowock, J., Seifried, C., Rüb, U., Walter, M. and Auburger, G. (2012) ATXN2-CAG42 Sequesters PABPC1 into insolubility and induces FBXW8 in cerebellum of old ataxic knock-in mice. *PLOS Genet.*, **8**, e1002920.
7. Kiehl, T.-R., Nechiporuk, A., Figueroa, K.P., Keating, M.T., Huynh, D.P. and Pulst, S.-M. (2006) Generation and characterization of Sca2 (ataxin-2) knockout mice. *Biochem. Biophys. Res. Commun.*, **339**, 17–24.
8. Lastres-Becker, I., Brodesser, S., Lütjohann, D., Azizov, M., Buchmann, J., Hintermann, E., Sandhoff, K., Schürmann, A., Nowock, J. and Auburger, G. (2008) Insulin receptor and lipid metabolism pathology in ataxin-2 knock-out mice. *Hum. Mol. Genet.*, **17**, 1465–1481.
9. Huynh, D.P., Maalouf, M., Silva, A.J., Schweizer, F.E. and Pulst, S.M. (2009) Dissociated fear and spatial learning in mice with deficiency of ataxin-2. *PLoS One*, **4**, e6235.
10. Somvanshi, P.R. and Venkatesh, K.V. (2014) A conceptual review on systems biology in health and diseases: from biological networks to modern therapeutics. *Syst. Synth. Biol.*, **8**, 99–116.
11. Keifer, J. and Summers, C.H. (2016) Putting the 'biology' back into 'neurobiology': the strength of diversity in animal model systems for neuroscience research. *Front. Syst. Neurosci.*, **10**,
12. Huang, D.W., Sherman, B.T. and Lempicki, R.A. (2008) Systematic and integrative analysis of large gene lists using DAVID bioinformatics resources. *Nat. Protoc.*, **4**, 44–57.
13. Ashburner, M., Ball, C.A., Blake, J.A., Botstein, D., Butler, H., Cherry, J.M., Davis, A.P., Dolinski, K., Dwight, S.S., Eppig, J.T. *et al.* (2000) Gene ontology: tool for the unification of biology. *Nat. Genet.*, **25**, 25–29.
14. Rong, Y., Wang, T. and Morgan, J.I. (2004) Identification of candidate Purkinje cell-specific markers by gene expression profiling in wild-type and pcd3J mice. *Mol. Brain Res.*, **132**, 128–145.
15. Larvie, M., Shoup, T., Chang, W.-C., Chigweshe, L., Hartshorn, K., White, M.R., Stahl, G.L., Elmaleh, D.R., Takahashi, K., Larvie, M. *et al.* (2012) Mannose-binding lectin binds to amyloid β protein and modulates inflammation, mannose-binding lectin binds to amyloid β protein and modulates inflammation. *J. Biomed. Biotechnol.*, **2012**, e929803.
16. Langfelder, P. and Horvath, S. (2008) WGCNA: an R package for weighted correlation network analysis. *BMC Bioinformatics*, **9**, 559.
17. Zhang, B. and Horvath, S. (2005) A general framework for weighted gene co-expression network analysis. *Stat. Appl. Genet. Mol. Biol.*, **4**, Article17, 1–43.
18. Langfelder, P., Mischel, P.S. and Horvath, S. (2013) When is hub gene selection better than standard meta-analysis? *PLoS ONE*, **8**, e61505.
19. Langfelder, P. and Horvath, S. (2007) Eigengene networks for studying the relationships between co-expression modules. *BMC Syst. Biol.*, **1**, 54.
20. Stepanov, G.A., Filippova, J.A., Komissarov, A.B., Kuligina, E.V., Richter, V.A., Semenov, D.V., Stepanov, G.A., Filippova, J.A., Komissarov, A.B., Kuligina, E.V. *et al.* (2015) Regulatory role of small nucleolar RNAs in human diseases, regulatory role of small nucleolar RNAs in human diseases. *BioMed Res. Int.*, **2015**, e206849.
21. Papadopoulou, A.S., Serneels, L., Achsel, T., Mandemakers, W., Callaerts-Vegh, Z., Dooley, J., Lau, P., Ayoubi, T., Radaelli, E., Spinazzi, M. *et al.* (2015) Deficiency of the miR-29a/b-1 cluster leads to ataxic features and cerebellar alterations in mice. *Neurobiol. Dis.*, **73**, 275–288.
22. Agarwal, V., Bell, G.W., Nam, J.-W. and Bartel, D.P. (2015) Predicting effective microRNA target sites in mammalian mRNAs. *eLife*, **4**, e05005.
23. Friedman, R.C., Farh, K.K.-H., Burge, C.B. and Bartel, D.P. (2009) Most mammalian mRNAs are conserved targets of microRNAs. *Genome Res.*, **19**, 92–105.
24. Sethupathy, P., Corda, B. and Hatzigeorgiou, A.G. (2006) TarBase: a comprehensive database of experimentally supported animal microRNA targets. *rna*, **12**, 192–197.

25. Serra, H.G., Byam, C.E., Lande, J.D., Tousey, S.K., Zoghbi, H.Y. and Orr, H.T. (2004) Gene profiling links SCA1 pathophysiology to glutamate signaling in Purkinje cells of transgenic mice. *Hum. Mol. Genet.*, **13**, 2535–2543.
26. Chou, A.-H., Yeh, T.-H., Ouyang, P., Chen, Y.-L., Chen, S.-Y. and Wang, H.-L. (2008) Polyglutamine-expanded ataxin-3 causes cerebellar dysfunction of SCA3 transgenic mice by inducing transcriptional dysregulation. *Neurobiol. Dis.*, **31**, 89–101.
27. Friedrich, B., Euler, P., Ziegler, R., Kuhn, A., Landwehrmeyer, B.G., Luthi-Carter, R., Weiller, C., Hellwig, S. and Zucker, B. (2012) Comparative analyses of Purkinje cell gene expression profiles reveal shared molecular abnormalities in models of different polyglutamine diseases. *Brain Res.*, **1481**, 37–48.
28. Ingram, M., Wozniak, E.A.L., Duvick, L., Yang, R., Bergmann, P., Carson, R., O'Callaghan, B., Zoghbi, H.Y., Henzler, C. and Orr, H.T. (2016) Cerebellar transcriptome profiles of ATXN1 transgenic mice reveal SCA1 disease progression and protection pathways. *Neuron*, **89**, 1194–1207.
29. Luthi-Carter, R., Strand, A.D., Hanson, S.A., Kooperberg, C., Schilling, G., La Spada, A.R., Merry, D.E., Young, A.B., Ross, C.A., Borchelt, D.R. *et al.* (2002) Polyglutamine and transcription: gene expression changes shared by DRPLA and Huntington's disease mouse models reveal context-independent effects. *Hum. Mol. Genet.*, **11**, 1927–1937.
30. Evert, B.O., Vogt, I.R., Vieira-Saecker, A.M., Ozimek, L., de Vos, R.A.I., Brunt, E.R.P., Klockgether, T. and Wüllner, U. (2003) Gene expression profiling in ataxin-3 expressing cell lines reveals distinct effects of normal and mutant ataxin-3. *J. Neuropathol. Exp. Neurol.*, **62**, 1006–1018.
31. Lucas, E.K., Reid, C.S., McMeekin, L.J., Dougherty, S.E., Floyd, C.L. and Cowell, R.M. (2015) Cerebellar transcriptional alterations with Purkinje cell dysfunction and loss in mice lacking PGC-1Î±. *Front. Cell. Neurosci.*, **8**, 441.
32. Meera, P., Pulst, S.M. and Otis, T.S. (2016) Cellular and circuit mechanisms underlying spinocerebellar ataxias. *J. Physiol.*, **594**, 4653–4660.
33. Chen, X., Tang, T.-S., Tu, H., Nelson, O., Pook, M., Hammer, R., Nukina, N. and Bezprozvanny, I. (2008) Deranged calcium signaling and neurodegeneration in spinocerebellar ataxia type 3. *J. Neurosci. Off. J. Soc. Neurosci.*, **28**, 12713.
34. Liu, J., Tang, T.-S., Tu, H., Nelson, O., Herndon, E., Huynh, D.P., Pulst, S.-M. and Bezprozvanny, I. (2009) Deranged calcium signaling and neurodegeneration in spinocerebellar ataxia type 2. *J. Neurosci. Off. J. Soc. Neurosci.*, **29**, 9148.
35. Watase, K., Barrett, C.F., Miyazaki, T., Ishiguro, T., Ishikawa, K., Hu, Y., Unno, T., Sun, Y., Kasai, S., Watanabe, M. *et al.* (2008) Spinocerebellar ataxia type 6 knockin mice develop a progressive neuronal dysfunction with age-dependent accumulation of mutant CaV2.1 channels. *Proc. Natl. Acad. Sci. U.S.A.*, **105**, 11987–11992.
36. Mark, M.D., Schwitalla, J.C., Groemmke, M. and Herlitze, S. Keeping our calcium in balance to maintain our balance. *Biochem. Biophys. Res. Commun.*, doi:10.1016/j.bbrc.2016.07.020.
37. van de Leemput, J., Chandran, J., Knight, M.A., Holtzclaw, L.A., Scholz, S., Cookson, M.R., Houlden, H., Gwinn-Hardy, K., Fung, H.-C., Lin, X. *et al.* (2007) Deletion at ITPR1 underlies ataxia in mice and spinocerebellar ataxia 15 in humans. *PLoS Genet.*, **3**, e108.
38. Yabe, I., Sasaki, H., Chen, D.-H., Raskind, W.H., Bird, T.D., Yamashita, I., Tsuji, S., Kikuchi, S. and Tashiro, K. (2003) Spinocerebellar ataxia type 14 caused by a mutation in protein kinase C gamma. *Arch. Neurol.*, **60**, 1749–1751.
39. Huynh, D.P., Yang, H.-T., Vakharia, H., Nguyen, D. and Pulst, S.M. (2003) Expansion of the polyQ repeat in ataxin-2 alters its Golgi localization, disrupts the Golgi complex and causes cell death. *Hum. Mol. Genet.*, **12**, 1485–1496.
40. Yoo, S.Y., Pennesi, M.E., Weeber, E.J., Xu, B., Atkinson, R., Chen, S., Armstrong, D.L., Wu, S.M., Sweatt, J.D. and Zoghbi, H.Y. (2003) SCA7 knockin mice model human SCA7 and reveal gradual accumulation of mutant ataxin-7 in neurons and abnormalities in short-term plasticity. *Neuron*, **37**, 383–401.
41. Crespo-Barreto, J., Fryer, J.D., Shaw, C.A., Orr, H.T. and Zoghbi, H.Y. (2010) Partial loss of ataxin-1 function contributes to transcriptional dysregulation in spinocerebellar ataxia type 1 pathogenesis. *PLoS Genet*, **6**, e1001021.
42. Miller, J.A., Woltjer, R.L., Goodenbour, J.M., Horvath, S. and Geschwind, D.H. (2013) Genes and pathways underlying regional and cell type changes in Alzheimer's disease. *Genome Med.*, **5**, 48.
43. Fogel, B.L., Cho, E., Wahnich, A., Gao, F., Becherel, O.J., Wang, X., Fike, F., Chen, L., Criscuolo, C. D., Michele, G. *et al.* (2014) Mutation of senataxin alters disease-specific transcriptional networks in patients with ataxia with oculomotor apraxia type 2. *Hum. Mol. Genet.*, **23**, 4758–4769.
44. Bettencourt, C., Forabosco, P., Wiethoff, S., Heidari, M., Johnstone, D.M., Botía, J.A., Collingwood, J.F., Hardy, J., Milward, E.A., Ryten, M. *et al.* (2016) Gene co-expression networks shed light into diseases of brain iron accumulation. *Neurobiol. Dis.*, **87**, 59–68.
45. Provenzano, G., Corradi, Z., Monsorno, K., Fedrizzi, T., Ricceri, L., Scattoni, M.L. and Bozzi, Y. (2016) Comparative gene expression analysis of two mouse models of autism: transcriptome profiling of the BTBR and En2 (−/−) hippocampus. *Front. Neurosci.*, **10**, 396.
46. Maciotta, S., Meregalli, M. and Torrente, Y. (2013) The involvement of microRNAs in neurodegenerative diseases. *Front. Cell. Neurosci.*, **7**, 265.
47. Rodriguez-Lebron, E., Liu, G., Keiser, M., Behlke, M.A. and Davidson, B.L. (2013) Altered Purkinje cell miRNA expression and SCA1 pathogenesis. *Neurobiol. Dis.*, **54**, 456–463.
48. Liang, J., Xing, D., Li, Z., Shen, J., Zhao, H. and Li, S. (2016) TRIM59 is upregulated and promotes cell proliferation and migration in human osteosarcoma. *Mol. Med. Rep.*, **13**, 5200–5206.
49. Zhan, W., Han, T., Zhang, C., Xie, C., Gan, M., Deng, K., Fu, M. and Wang, J.-B. (2015) TRIM59 promotes the proliferation and migration of non-small cell lung cancer cells by upregulating cell cycle related proteins. *PLoS One*, **10**, e0142596.
50. Nakatani, J., Tamada, K., Hatanaka, F., Ise, S., Ohta, H., Inoue, K., Tomonaga, S., Watanabe, Y., Chung, Y.J., Banerjee, R. *et al.* (2009) Abnormal behavior in a chromosome-engineered mouse model for human 15q11-13 duplication seen in autism. *Cell*, **137**, 1235–1246.
51. Persengiev, S., Kondova, I., Otting, N., Koeppen, A.H. and Bontrop, R.E. (2011) Genome-wide analysis of miRNA expression reveals a potential role for miR-144 in brain aging and spinocerebellar ataxia pathogenesis. *Neurobiol. Aging*, **32**, 2316.e17–2316.e27.
52. Betel, D., Koppal, A., Agius, P., Sander, C. and Leslie, C. (2010) Comprehensive modeling of microRNA targets predicts functional non-conserved and non-canonical sites. *Genome Biol.*, **11**, R90.
53. Hu, Z., Mellor, J., Wu, J. and DeLisi, C. (2004) VisANT: an online visualization and analysis tool for biological interaction data. *BMC Bioinformatics*, **5**, 17.